

NASA Technical Memorandum 106721
ICOMP-94-21; CMOTT-94-6

11-57
22322
32P

A New k - ϵ Eddy Viscosity Model for High Reynolds Number Turbulent Flows—Model Development and Validation

T.-H. Shih, W.W. Liou, A. Shabbir, Z. Yang, and J. Zhu
*Institute for Computational Mechanics in Propulsion
and Center for Modeling of Turbulence and Transition
Lewis Research Center
Cleveland, Ohio*

(NASA-TM-106721) A NEW K-EPSILON
EDDY VISCOSITY MODEL FOR HIGH
REYNOLDS NUMBER TURBULENT FLOWS:
MODEL DEVELOPMENT AND VALIDATION
(NASA. Lewis Research Center) 32 p

N95-11442

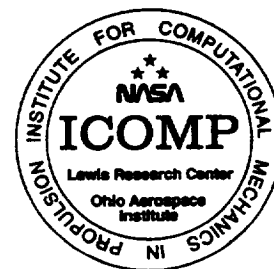
Unclass

G3/34 0022322

August 1994



National Aeronautics and
Space Administration





A New k - ϵ Eddy Viscosity Model for High Reynolds Number Turbulent Flows—Model Development and Validation

T.-H. Shih, W. W. Liou, A. Shabbir, Z. Yang and J. Zhu

Center for Modeling of Turbulence and Transition
and Institute for Computational Mechanics in Propulsion
NASA Lewis Research Center, Cleveland, OH 44135

Abstract

A new k - ϵ eddy viscosity model, which consists of a new model dissipation rate equation and a new realizable eddy viscosity formulation, is proposed in this paper. The new model dissipation rate equation is based on the dynamic equation of the mean-square vorticity fluctuation at large turbulent Reynolds number. The new eddy viscosity formulation is based on the realizability constraints; the positivity of normal Reynolds stresses and Schwarz' inequality for turbulent shear stresses. We find that the present model with a set of unified model coefficients can perform well for a variety of flows. The flows that are examined include: (i) rotating homogeneous shear flows; (ii) boundary-free shear flows including a mixing layer, planar and round jets; (iii) a channel flow, and flat plate boundary layers with and without a pressure gradient; and (iv) backward facing step separated flows. The model predictions are compared with available experimental data. The results from the standard k - ϵ eddy viscosity model are also included for comparison. It is shown that the present model is a significant improvement over the standard k - ϵ eddy viscosity model.

1. Introduction

The main task in developing a k - ε eddy viscosity model is to provide an appropriate eddy viscosity formulation and a model dissipation rate equation. The standard k - ε eddy viscosity model, which is widely used in computational fluid dynamics, performs quite well for boundary layer flows but not for flows with a high mean shear rate or a massive separation, because in these cases the eddy viscosity is overpredicted by the standard eddy viscosity formulation. In addition, the standard model dissipation rate equation does not always give the appropriate length scale for turbulence. For example, the well-known anomaly about the spreading rate of a planar jet versus a round jet is mainly due to the model dissipation rate equation. In order to improve the ability of the k - ε eddy viscosity model to predict complex turbulent flows, these deficiencies in the existing k - ε eddy viscosity model should be removed. The purpose of this study is to propose new formulations for both the model dissipation rate equation and the eddy viscosity that can significantly improve the performance of the k - ε eddy viscosity model.

The exact dissipation rate equation can be written as,

$$\begin{aligned} \varepsilon_{,t} + U_i \varepsilon_{,i} = & \nu \varepsilon_{,ii} - (\overline{\varepsilon' u_i})_{,i} - \frac{2\nu}{\rho} (\overline{p_{,k} u_{i,k}})_{,i} \\ & - 2\nu \overline{u_j u_{i,k}} U_{i,kj} - 2\nu \overline{u_{i,k} u_{j,k}} U_{i,j} - 2\nu \overline{u_{i,j} u_{i,k}} U_{j,k} \\ & - 2\nu \overline{u_{i,k} u_{j,k} u_{i,j}} - 2\nu^2 \overline{u_{i,jk} u_{i,jk}} \end{aligned} \quad (1a)$$

where $\varepsilon = \nu \overline{u_{i,j} u_{i,j}}$, $\varepsilon' = \nu u_{i,j} u_{i,j}$ and $()_{,t}$, $()_{,i}$ stand for the derivatives with respect to t and x_i . All the terms on the right hand side of Eq. (1a), except the viscous diffusion term $\nu \varepsilon_{,ii}$, are new unknowns. Thus, they must be modeled before this equation can be used for applications. Modeling of these new unknowns, which are related to the small scales of turbulence, is extremely difficult. Therefore, in the literature, Eq. (1a) is usually not considered as a useful equation to work with. Instead, one creates a simple model dissipation rate equation which has a structure similar to that of the turbulent kinetic energy equation. That is, the dissipation rate equation also has generation and destruction terms which are assumed to be proportional to the production and dissipation of turbulent kinetic energy divided by the large eddy turn-over time, k/ε . With this assumption, the resulting model dissipation rate equation can be written in the following form:

$$\varepsilon_{,t} + U_i \varepsilon_{,i} = \nu \varepsilon_{,ii} - (\overline{\varepsilon' u_i})_{,i} - C_{\varepsilon 1} \frac{\varepsilon}{k} \overline{u_i u_j} U_{i,j} - C_{\varepsilon 2} \frac{\varepsilon^2}{k} \quad (1b)$$

Eq.(1b) is the standard form of the model dissipation rate equation which has been widely used in various turbulence closure schemes. In addition, several modified versions of Eq.(1b) have also been proposed for different applications, for example, in near-wall turbulent flows¹⁻⁴ and in rotating turbulent flows⁵. Recently, Lumley⁶ proposed a dissipation rate equation based on the concept of non-equilibrium spectral energy transfer due to the interactions between eddies of different sizes. A new transport equation for an inverse time scale has also been suggested in conjunction with his new ε equation which is of a different form from that of Eq.(1b). This model mimics the physics of the statistical energy transfer from large eddies to small eddies and was successful in the prediction of some turbulent free shear flows⁶. In the present study, we explore the possibility of deriving a new model form for the dissipation rate equation which is not only physically more related to the original ε equation but also simpler and more robust than the standard dissipation equation (1b). This is achieved by first developing a model equation for the dynamic equation of the mean-square vorticity fluctuation $\overline{\omega_i \omega_i}$. Once the dynamic equation for $\overline{\omega_i \omega_i}$ is modeled, a model dissipation rate equation can be readily obtained by using the relation $\varepsilon = \nu \overline{\omega_i \omega_i}$ at large Reynolds number.

The standard eddy viscosity formulation for incompressible turbulence is

$$-\overline{u_i u_j} = -\frac{2}{3} k \delta_{ij} + \nu_T (U_{i,j} + U_{j,i}) \quad (2a)$$

$$\nu_T = C_\mu \frac{k^2}{\varepsilon} \quad (2b)$$

$$C_\mu = 0.09 \quad (2c)$$

It has been known for long that this model will become non-realizable in the case of large mean strain rate (e.g., $Sk/\varepsilon > 3.7$ where $S = \sqrt{2S_{ij}S_{ij}}$), because the normal stresses can become negative and Schwarz' inequality for shear stresses can be violated. To insure realizability, the model coefficient C_μ must not be a constant and must be related to the mean strain rate. In fact, the experiments on boundary layer and homogeneous shear flows also show that the value of C_μ is quite different in each case. For example, C_μ is about 0.09 in the inertial sublayer of a flat boundary layer in which $Sk/\varepsilon = 3.3$, and C_μ is about 0.05 in a homogeneous shear flow of $Sk/\varepsilon = 6$. According to the above considerations, a new formulation for C_μ , which was suggested by Reynolds⁷ and Shih *et al.*⁸, is adopted in this paper.

In the following sections, we will first describe the development of a new model dis-

sipation rate equation, and then the development of the new eddy viscosity formulation. The performance of the new model will be examined in a variety of flows which include rotating homogeneous shear flows, boundary-free shear flows (e.g., a mixing layer, planar and round jets), a channel flow, boundary layers with and without pressure gradients, and backward facing step separated flows.

2. Development of the new dissipation rate equation

2.1 Dynamic equation for $\overline{\omega_i \omega_i}$

The exact equation for $\overline{\omega_i \omega_i}$ is

$$\begin{aligned} \left(\frac{\overline{\omega_i \omega_i}}{2}\right)_{,t} + U_j \left(\frac{\overline{\omega_i \omega_i}}{2}\right)_{,j} &= \nu \left(\frac{\overline{\omega_i \omega_i}}{2}\right)_{,jj} - \frac{1}{2} (\overline{u_j \omega_i \omega_i})_{,j} \\ &+ \overline{\omega_i u_{i,j}} \Omega_j - \overline{u_j \omega_i} \Omega_{i,j} + \overline{\omega_i \omega_j} U_{i,j} \\ &+ \overline{\omega_i \omega_j u_{i,j}} - \nu \overline{\omega_{i,j} \omega_{i,j}} \end{aligned} \quad (3)$$

where u_i and U_i are the fluctuating and mean velocities, and ω_i and Ω_i are the fluctuating and mean vorticities which are defined by

$$\omega_i = \epsilon_{ijk} u_{k,j}, \quad \Omega_i = \epsilon_{ijk} U_{k,j} \quad (4)$$

and

$$S_{ij} = \frac{1}{2} (U_{i,j} + U_{j,i}), \quad \Omega_{ij} = \frac{1}{2} (U_{i,j} - U_{j,i})$$

Tennekes and Lumley⁹ clearly described the physical meaning of each term in Eq.(3). The first two terms on the right hand side represent the viscous transport and the turbulent transport of $\overline{\omega_i \omega_i}$, respectively. The third term is the source term which is produced by fluctuating vortex stretching and mean vorticity. This term also appears in the equation for $\Omega_i \Omega_i$ with the same sign, hence, it will either increase or decrease $\Omega_i \Omega_i$ and $\overline{\omega_i \omega_i}$ simultaneously. The fourth term represents the vorticity exchange between $\overline{\omega_i \omega_i}$ and $\Omega_i \Omega_i$, because it appears with opposite sign in the equation for $\Omega_i \Omega_i$. The fifth term represents the source produced by mean vortex stretching. The sixth and seventh terms are the production due to fluctuating vortex stretching and the dissipation due to the viscosity of the fluid, respectively. Tennekes and Lumley have shown that, at sufficiently high turbulent Reynolds numbers, the sixth and the seventh terms in Eq.(3) are the largest terms and are of order:

$$\overline{\omega_i \omega_j u_{i,j}}, \nu \overline{\omega_{i,j} \omega_{i,j}} \approx \mathcal{O}\left(\frac{u^3}{l^3} R_t^{3/2}\right)$$

All the remaining terms on the right hand side, except the second term, are smaller, either of order (u^3/l^3) or $(u/l)^3 R_t^{\frac{1}{2}}$. In the above analysis, “ \mathcal{O} ” denotes the order of magnitude, $R_t = ul/\nu$ is the turbulent Reynolds number, and u and l are the characteristic velocity and length scales of turbulence, respectively. If the terms of order $(u^3/l^3)R_t$ or larger were kept in Eq.(3), then the evolution of $\overline{\omega_i \omega_i}$ would be described by the following equation,

$$\left(\frac{\overline{\omega_i \omega_i}}{2}\right)_{,t} + U_j \left(\frac{\overline{\omega_i \omega_i}}{2}\right)_{,j} = -\frac{1}{2}(\overline{u_j \omega_i \omega_i})_{,j} + \overline{\omega_i \omega_j u_{i,j}} - \nu \overline{\omega_{i,j} \omega_{i,j}} \quad (5)$$

As pointed out by Tennekes and Lumley, at very large Reynolds numbers, Eq.(5) becomes,

$$\overline{\omega_i \omega_j u_{i,j}} = \nu \overline{\omega_{i,j} \omega_{i,j}} \quad (6)$$

Or equivalently, production equals dissipation. This relation indicates that the term $\overline{\omega_i \omega_j u_{i,j}}$ is always positive. In addition, it indicates that there is a new length scale created by the vortex stretching which is related to the derivative of fluctuating vorticity. The vortex stretching tends to reduce the size of eddies and to create a broad spectrum of eddy sizes. However, this process must end at a certain level of eddy size because of the smoothing effect of viscosity. We expect that the terminal eddy size is the Kolmogorov microscale which corresponds to the length scale for the derivative of fluctuating vorticity $\omega_{i,j}$. This can be easily verified from Eq.(6).

2.2 Modeling of the dynamic equation for $\overline{\omega_i \omega_i}$

Modeling of $\overline{\omega_i \omega_j u_{i,j}}$. We first define a fluctuating anisotropic tensor b_{ij}^ω using $\omega_i \omega_j$

$$b_{ij}^\omega = \frac{\omega_i \omega_j}{\omega_k \omega_k} - \frac{1}{3} \delta_{ij} \quad (7)$$

then

$$\overline{\omega_i \omega_j u_{i,j}} = \overline{b_{ij}^\omega \omega_k \omega_k u_{i,j}} \quad (8)$$

We expect that the vortex stretching tends to align vortex lines with the strain rate and that the anisotropy b_{ij}^ω is mainly due to the anisotropy of the fluctuating strain rate; hence, the anisotropy b_{ij}^ω may be assumed to be proportional to the strain rate s_{ij} . That is,

$$b_{ij}^\omega \propto \frac{s_{ij}}{s}, \quad (9)$$

where

$$s = (2s_{ij}s_{ij})^{1/2}, \quad s_{ij} = (u_{i,j} + u_{j,i})/2$$

This leads to

$$\overline{\omega_i \omega_j u_{i,j}} \propto \overline{\omega_k \omega_k} \frac{\overline{s_{ij} u_{i,j}}}{s} \propto \overline{\omega_k \omega_k} s \quad (10)$$

If we further assume that $\overline{\omega_k \omega_k}$ and $(2s_{ij} s_{ij})^{1/2}$ are well correlated, we may write

$$\overline{\omega_i \omega_j u_{i,j}} \propto \overline{\omega_k \omega_k} \sqrt{2s_{ij} s_{ij}} \quad (11)$$

Noting that $\overline{\omega_i \omega_i} = 2\overline{s_{ij} s_{ij}}$ at large Reynolds numbers, we may also write

$$\overline{\omega_i \omega_j u_{i,j}} \propto \overline{\omega_k \omega_k} \sqrt{\overline{\omega_i \omega_i}} = \frac{\overline{\omega_k \omega_k} \overline{\omega_i \omega_i}}{\sqrt{\overline{\omega_i \omega_i}}} \quad (12)$$

Eqs.(11) and (12) both indicate that the model for $\overline{\omega_i \omega_j u_{i,j}}$ is of order $(u^3/\ell^3)R_t^{3/2}$ as it should be.

Modeling of $\overline{\omega_i \omega_j u_{i,j}} - \nu \overline{\omega_{i,j} \omega_{i,j}}$. Eq.(5) indicates that $\overline{\omega_i \omega_j u_{i,j}} - \nu \overline{\omega_{i,j} \omega_{i,j}}$ must be of order $(u^3/\ell^3)R_t$, because that is the order of the magnitude for the other terms in Eq.(5). Therefore, the model of $-\nu \overline{\omega_{i,j} \omega_{i,j}}$ must cancel $\overline{\omega_k \omega_k} \sqrt{2s_{ij} s_{ij}}$ (or $\overline{\omega_k \omega_k} \overline{\omega_i \omega_i} / \sqrt{\overline{\omega_i \omega_i}}$) in such a way that their difference is smaller than $\overline{\omega_k \omega_k} \sqrt{2s_{ij} s_{ij}}$ (or $\overline{\omega_k \omega_k} \overline{\omega_i \omega_i} / \sqrt{\overline{\omega_i \omega_i}}$) by an order of $R_t^{1/2}$. This suggests that the sum of these two terms can be related to the following two terms:

$$\overline{\omega_k \omega_k} S, \quad \frac{\overline{\omega_k \omega_k} \overline{\omega_i \omega_i}}{\frac{k}{\nu} + \sqrt{\overline{\omega_i \omega_i}}} \quad (13)$$

since both the ratio of s to S and the ratio of k/ν to $\sqrt{\overline{\omega_i \omega_i}}$ are of order $R_t^{1/2}$. Here, k ($\approx u^2$) denotes the turbulent kinetic energy and S is the mean strain rate ($\sqrt{2s_{ij} s_{ij}}$). As a result, the dynamic equation for fluctuating vorticity can be modeled as

$$\begin{aligned} \left(\frac{\overline{\omega_i \omega_i}}{2}\right)_{,t} + U_j \left(\frac{\overline{\omega_i \omega_i}}{2}\right)_{,j} &= -\frac{1}{2} (\overline{u_j \omega_i \omega_i})_{,j} + C_1 \overline{\omega_k \omega_k} S \\ &\quad - C_2 \frac{\overline{\omega_k \omega_k} \overline{\omega_i \omega_i}}{\frac{k}{\nu} + \sqrt{\overline{\omega_i \omega_i}}} \end{aligned} \quad (14)$$

Note that the denominator of the last term in Eq.(14) should be k/ν for large Reynolds number turbulence since the term $\sqrt{\overline{\omega_i \omega_i}}$ is negligible compared to k/ν . However, we keep it there in case k vanishes somewhere in the flow field to prevent unnecessary singularity. This also reflects the fact that the parent term of the model, Eq.(12), shows no singularity

anywhere in the flow field. It should also be pointed out that the sum of last two terms in Eq.(14) models the last two terms in Eq.(5) as a whole and should not be viewed as a model for either individual term.

2.3 Modeling of the dissipation rate equation

Noting that at large Reynolds number $\varepsilon = \nu \overline{\omega_i \omega_i}$ and multiplying Eq.(14) by ν , we readily obtain a modeled dissipation rate equation,

$$\varepsilon_{,t} + U_j \varepsilon_{,j} = -(\overline{u_j \varepsilon'})_{,j} + C_1 S \varepsilon - C_2 \frac{\varepsilon^2}{k + \sqrt{\nu \varepsilon}} \quad (15)$$

The model coefficients, C_1 and C_2 , are expected to be independent of the Reynolds number as the Reynolds number becomes large. We note that C_1 and C_2 may be affected by solid body rotation imposed on turbulence through the reduction of fluctuation vortex stretching, $\overline{\omega_i \omega_j u_{i,j}}$, as was shown by Bardina⁵; however, this effect is rather weak compared to the other mechanisms. For example, Reynolds stresses will first be substantially affected by rotation and result in a substantial change of the turbulent field, say k , as shown in the calculation of the rotating homogeneous shear flows in section 4.1. This will also affect the evolution of ε through, say, k . The signs of C_1 and C_2 can be easily determined. For example, in a decaying grid turbulence, only the last term on the right hand side of Eq.(15) is non-zero and must be negative, hence C_2 must be positive. For the case of homogeneous shear flow, both the turbulent kinetic energy and its dissipation rate increase with time so that the “source” term in Eq.(15) must be positive, hence C_1 must be positive. In fact, these two types of flows^{10,11} will be used for determining the coefficients C_1 and C_2 .

The difference between the present model dissipation rate equation, Eq.(15), and the standard model dissipation rate equation, Eq.(1b), is the “source” term. The Reynolds stresses do not appear in Eq.(15). Consequently, the present model dissipation rate equation will be more robust than the standard model dissipation rate equation when it is used in conjunction with second-order closure schemes, since S normally behaves better than the Reynolds stresses in numerical calculations, especially for cases with poor initial conditions. In addition, the present form of the “production” term is similar to that proposed by Lumley⁶ which is based on the concept of spectral energy transfer. We believe that the present form of the model dissipation rate equation describes the turbulent vortex stretching and dissipation terms more appropriately.

Eq.(15) can be applied in conjunction with any level of turbulence closure; however, the turbulent transport term $(\overline{\varepsilon'u_i})_{,i}$ needs to be modeled differently at different levels of turbulence closure. Here, we apply Eq.(15) to a realizable eddy viscosity model which will be described in the next section, and where $(\overline{\varepsilon'u_i})_{,i}$ is modeled as

$$(\overline{\varepsilon'u_i})_{,i} = -\left(\frac{\nu_T}{\sigma_\varepsilon}\varepsilon_{,i}\right)_{,i} \quad (16)$$

The model coefficients C_1, C_2 and σ_ε will be determined later.

3. Realizable eddy viscosity model

Shih *et al.*⁸ proposed a realizable Reynolds stress algebraic equation model. Its linear form represents an isotropic eddy viscosity model:

$$-\overline{u_i u_j} = \nu_T(U_{i,j} + U_{j,i}) - \frac{2}{3}k\delta_{ij} \quad (17.1)$$

$$\nu_T = C_\mu \frac{k^2}{\varepsilon} \quad (17.2)$$

Here the coefficient C_μ is not a constant. The experimental as well as DNS data on the inertial sublayer of a channel or boundary layer flow suggest that $C_\mu = 0.09$. On the other hand, for a homogeneous shear flow, $C_\mu = -\frac{\overline{uv}}{k} / \frac{k}{\varepsilon} \frac{\partial U}{\partial y}$ which is about 0.05 from the experiment of Tavoularis and Corrsin¹¹. Based on the realizability conditions:

$$\begin{aligned} \overline{u_\alpha^2} &\geq 0 \quad (\alpha = 1, 2, 3) \\ \frac{\overline{u_\alpha u_\beta^2}}{\overline{u_\alpha^2} \overline{u_\beta^2}} &\leq 1 \quad (\alpha = 1, 2, 3; \beta = 1, 2, 3) \end{aligned} \quad (18)$$

Reynolds⁷ and Shih *et al.*⁸ proposed the following formulation for the coefficient of C_μ :

$$C_\mu = \frac{1}{A_0 + A_s U^{(*)} \frac{k}{\varepsilon}} \quad (19)$$

In the formulation of Shih *et al.*⁸,

$$\begin{aligned} U^{(*)} &= \sqrt{S_{ij}S_{ij} + \tilde{\Omega}_{ij}\tilde{\Omega}_{ij}} \\ \tilde{\Omega}_{ij} &= \Omega_{ij} - 2\epsilon_{ijk}\omega_k \\ \Omega_{ij} &= \overline{\Omega}_{ij} - \epsilon_{ijk}\omega_k \end{aligned} \quad (20)$$

where $\overline{\Omega_{ij}}$ is the mean rotation rate viewed in a rotating reference frame with the angular velocity ω_k . The parameter A_s is determined by

$$\begin{aligned} A_s &= \sqrt{6} \cos \phi, \quad \phi = \frac{1}{3} \arccos(\sqrt{6}W) \\ W &= \frac{S_{ij}S_{jk}S_{ki}}{\tilde{S}^3} \quad \tilde{S} = \sqrt{S_{ij}S_{ij}} \end{aligned} \quad (21)$$

Calibration of the model coefficient A_0 . The new eddy viscosity formulation of Eqs.(17), (19), (20) and (21) satisfies the realizability constraints Eq.(18), and hence is a realizable model. The only undetermined coefficient is A_0 . If we assume for simplicity that A_0 is a constant, then the value of A_0 can be calibrated by one of the simple flows, such as a homogeneous shear flow or a boundary layer flow. Here, we choose a boundary layer flow in hope that the model will be able to reproduce the log-law of the inertial sublayer. This leads to $A_0 = 4.0$ which corresponds to $C_\mu = 0.09$ in the inertial sublayer. For the homogeneous shear flow of Tavoularis and Corrsin¹¹, Eq.(19), with $A_0 = 4.0$, gives $C_\mu = 0.06$ which is much closer to the experimental value of 0.05 than that of the standard $C_\mu = 0.09$. The component of the anisotropy b_{12} ($\overline{uv}/2k$) for both the flows is listed in Table 1 which shows that the present form of C_μ also produces reasonable b_{12} compared to the standard form of C_μ .

Table 1. Anisotropy component b_{12}

	exp.	standard	present
boundary layer b_{12}	-0.149	-0.149	-0.149
homoge. shear b_{12}	-0.142	-0.274	-0.18

Now let us go back to the modeled k and ε equations,

$$k_{,t} + U_j k_{,j} = \left(\frac{\nu_T}{\sigma_k} k_{,j} \right)_{,j} - \overline{u_i u_j} U_{i,j} - \varepsilon \quad (22)$$

$$\varepsilon_{,t} + U_j \varepsilon_{,j} = \left(\frac{\nu_T}{\sigma_\varepsilon} \varepsilon_{,j} \right)_{,j} + C_1 S \varepsilon - C_2 \frac{\varepsilon^2}{k + \sqrt{\nu \varepsilon}} \quad (23)$$

and determine the coefficients in Eq.(23).

Calibration of the model coefficients C_1 , C_2 and σ_ε . In decaying grid turbulence at large Reynolds number, the equations for turbulent kinetic energy k and its

dissipation rate ε are

$$k_{,t} = -\varepsilon, \quad \varepsilon_{,t} = -C_2 \frac{\varepsilon^2}{k}$$

Let

$$\frac{k}{k_0} = \left(\frac{t}{t_0}\right)^{-n}, \quad \frac{\varepsilon}{\varepsilon_0} = \left(\frac{t}{t_0}\right)^{-\alpha}$$

the following equations can be obtained from the k and ε equations:

$$\alpha = n + 1, \quad C_2 = \frac{n + 1}{n} \quad (24)$$

Experiments¹⁰ show that the decay exponent n varies from 1.08 to 1.30. In this study we choose $C_2 = 1.9$ which corresponds to $n = 1.11$. After C_2 is chosen, we use the experimental data of homogeneous shear flow¹¹ and boundary layer flow to determine the coefficient C_1 which is found to be a simple function of the time scale ratio of the turbulence to the mean strain, η :

$$C_1 = \max\{0.43, \frac{\eta}{5 + \eta}\} \quad (25)$$

where

$$\eta = \frac{Sk}{\varepsilon}, \quad S = \sqrt{2S_{ij}S_{ij}}$$

The value of σ_ε will be estimated using the log-law in a boundary layer flow. The following relations hold in the inertial sublayer:

$$\begin{aligned} \frac{U}{u_\tau} &= \frac{1}{\kappa} \log \frac{u_\tau y}{\nu} + C \\ -\overline{uv} &\approx u_\tau^2, \quad -\overline{uv} \frac{\partial U}{\partial y} \approx \varepsilon \end{aligned} \quad (26)$$

Analyzing the dissipation rate equation in the log-law region, we obtain

$$\sigma_\varepsilon = \frac{\kappa^2}{C_2 \sqrt{C_\mu} - C_1} = 1.20 \quad (28)$$

where the von Karman constant $\kappa = 0.41$. The model coefficients are summarized in Table 2.

Table 2. Model coefficients

σ_k	σ_ε	C_1	C_2	C_μ	A_0
1.0	1.2	Eq.(25)	1.9	Eq.(19)	4.0

4. Model applications

The results of turbulent flow calculations using the proposed new turbulence model are shown in this section. These include (i) rotating homogeneous shear flows, (ii) boundary-free shear flows, (iii) a channel flow and boundary layers with and without pressure gradients, and (v) backward-facing step flows. The results of the present and the standard $k - \epsilon$ models are compared with DNS, LES and experiments.

4.1 Rotating homogeneous shear flows

The comparisons are made with the large eddy simulation of Bardina *et al.*⁵ for four different cases of Ω/S (which are $\Omega/S=0.0$, $\Omega/S=-0.50$, $\Omega/S=0.25$, and $\Omega/S=0.50$). The initial conditions in all these cases correspond to isotropic turbulence and $\epsilon_0/Sk_0 = 0.296$. Figure 1 (a) compares the evolution of turbulence kinetic energy, normalized by its initial value k_0 , with the non-dimensional time St for the case of $\Omega/S = 0.0$. For this case both the present and the standard $k - \epsilon$ (denoted by ske hereafter) models show the trends exhibited by LES, with the present model closer to the LES data. Figure 1 (b) shows the comparisons for the case $\Omega/S = 0.25$. The LES shows that the growth rate of the turbulence kinetic energy is increased over the no rotation rate case. The present model is able to pick up this trend while the ske model does not. Figures 1 (c) and 1 (d) compare the evolution of turbulence kinetic energy for two more cases of $\Omega/S = 0.5$ and $\Omega/S = -0.5$. For the first of these cases the LES shows that the growth rate of the turbulence kinetic energy is decreased over the no rotation rate case. The present model is able to pick up this trend and although the agreement between the present model and the LES is not as good as it is for the other cases, it still is a lot better than the ske model. For the case of $\Omega/S = -0.5$ the ske model does not show the effect of rotation on turbulence as it gives the same growth rate of turbulence kinetic energy as it did for the no rotation case, a result which is already known. On the other hand the present model is in reasonable agreement with the LES data as it shows the decay of the turbulence kinetic energy with time.

4.2 Boundary-free shear flows

Calculations using the present and the ske models were performed for a mixing layer, a planar and a round jet. Figures 2, 3 and 4 show the comparisons of the self-similar profiles from the model predictions and the various measurements for the mixing layer,

planar and round jets, respectively. In these figures, the profiles for the mean velocity the Reynolds shear stress and the turbulent kinetic energy are presented. For the mixing layer, the results are shown in a self-similar coordinate η defined as

$$\eta = -\frac{y - y_{0.5}}{y_{0.9} - y_{0.1}}$$

where $y_{0.1}$, $y_{0.5}$, and $y_{0.9}$ denote the locations where the ratio of the local mean velocity to that of the free stream are 0.1, 0.5, and 0.9, respectively. Figure 2 shows that the mean velocity profiles of the mixing layer predicted by either the present model or the ske model agree well with experimental data of Patel¹². The present model, however, gives better predictions of the turbulent kinetic energy and the Reynolds shear stress distributions than the ske model. This is especially true for their peak levels. The predictions for the planar jet are shown in Figure 3. The model predictions are compared with the measurements of Gutmark and Wygnanski¹³, Bradbury¹⁴, and Hekestad¹⁵. The predictions given by both the present model and the ske model agree well with the experimental data. The turbulent kinetic energy level at the jet centerline is slightly lower than the measured values. For the round jet, the comparisons are made between the model predictions and the measurements of Wygnanski and Fielder¹⁶ and Rodi¹⁷ and are shown in Figure 4. The profile distributions of the mean velocity predicted by the current model agree well with the experimental data, while the ske model predicts a much wider distribution. Significant improvement is also achieved in the prediction of the turbulent shear stress profile over the ske model in terms of both the centerline level and the overall distribution. The calculated spreading rates of these flows are compared with measurements and are shown in Table 3. The present model yields better predictions than the ske model; especially, the well-known spreading rate anomaly of planar and round jets (i.e., the measured spreading rate of a round jet is always smaller than that of a planar jet, but the model prediction usually contradicts the measurements) is removed completely.

Table 3. The spreading rates of turbulent free shear flows

Case	measurement	ske	present
mixing layer	0.13-0.17	0.152	0.151
planar jet	0.105-0.11	0.109	0.105
round jet	0.085-0.095	0.116	0.094

4.3 Channel flow and boundary layer flows

Turbulent channel flow and boundary layer flows with/without pressure gradients were calculated to test the performance of the present model for wall bounded flows. Since the present model is proposed for turbulent flows away from the wall, the integration was carried out down to $y^+ = 80$, rather than to the wall, in the calculations. At $y^+ = 80$, DNS values were used as the boundary conditions for the turbulent channel flow and wall functions were used for the turbulent boundary layer flows.

The velocity profile for 2D fully developed turbulent channel flow at $Re_\tau = 395$ is shown in Figure 5. This flow was calculated by Kim¹⁸ using direct numerical simulation. Both the present model and the ske model agree reasonably well with the DNS data. Figure 6 shows the skin friction coefficient for the flat plate boundary layers with the Reynolds number up to $Re_\theta = 16000$. Here, comparison is made with the experimental results of Wieghardt¹⁹. Both the present model and the ske model give good agreement with the experiments. Overall, the present model gives a slightly better prediction for boundary layer development.

Figure 7 shows the results for the Herring and Norbury flow²⁰, which is a boundary layer flow under favorable pressure gradient. The present model gives comparable performance to that of the ske model. The turbulent boundary layer under adverse pressure gradient studied by Bradshaw²¹ and the turbulent boundary layer under increasingly adverse pressure gradient studied by Samuel and Joubert²² were also calculated. The results are shown in Figure 8 and Figure 9, respectively. In both cases, the present model gives better predictions.

4.4 Backward-facing step flows

The performance of the present model for complex recirculating flows is demonstrated through calculations for two backward-facing step flows, one (DS-case²³) with smaller and the other (KKJ-case²⁴) with larger step height, both of which have been extensively used to benchmark calculations of separated flows. The calculations were performed with a conservative finite-volume procedure. The convection terms of the governing equations were discretized by a second-order accurate and bounded differencing scheme²⁵, and all the other terms by the standard central differencing scheme. Sufficiently fine grids, with

201×109 points in the DS-case and 199×91 points in the KKJ-case, were used to establish numerical credibility of the solutions. The computational domain had a length of 50 step heights, one fifth of which was placed upstream of the step. The experimental data were used to specify the inflow conditions, the fully-developed flow conditions were imposed at the outflow boundary, and the standard wall function approach²⁶ was used to bridge the viscous sublayer near the wall. Table 4 shows the comparison of the reattachment lengths. Figures 10-14 compare the skin friction, the pressure distribution along the bottom wall and the mean velocity as well as the turbulent stress profiles at three downstream locations. All the quantities were normalized by the step height h and the experimental reference free-stream velocity U_{ref} .

Table 4. Comparison of the reattachment point locations

Case	measurement	ske	present
DS	6.26	4.99	6.02
KKJ	7 ± 0.5	6.35	7.50

The comparison of the size of the separation bubble, the skin friction, and the pressure coefficients suggest that the overall performance of the present model is better than that of the ske model.

5. Concluding Remarks

A new $k-\epsilon$ eddy viscosity model is proposed in this paper. It consists of a new model dissipation rate equation and a new realizable eddy viscosity formulation. The new model dissipation rate equation is based on the dynamic equation for fluctuating vorticity. The new eddy viscosity formulation described in Section 3 ensures realizability and contains, as well, the effect of mean rotation on turbulence stresses. The present model is tested in various benchmark flows including: rotating homogeneous shear flows; boundary-free shear flows; channel and flat boundary layer flows with and without pressure gradients; and backward facing step flows. The results show that the present model performs better than the standard $k - \epsilon$ model in almost all the cases tested. The well-known spreading rate anomaly of planar and round jets is completely removed. In addition, the new model dissipation rate equation is expected to enhance the numerical stability in turbulent flow calculations, especially, when it is used in conjunction with more advanced closure schemes,

such as second order closures. We have also just finished implementing the present model dissipation rate equation into the LRR²⁷ second order closure. Preliminary results show that the initial decay behavior of k and ϵ and the effect of rotation on both k and ϵ for initially isotropic rotating homogeneous shear flows are well captured.

References

- ¹ Jones, W. P. and Launder, B. E., "The calculation of low-Reynolds number phenomena with a two-equation model of turbulence," *International Journal of Heat and Mass Transfer*, Vol. 16, 1973, pp. 1119-1130.
- ² Chien, K. Y., "Predictions of Channel and boundary layer flow with a low-Reynolds-number turbulence model," *AIAA Journal*, Vol. 20, 1982, pp. 33-38.
- ³ Yang, Z. and Shih, T.-H., "A new time scale based $k - \epsilon$ model for near wall turbulence," *AIAA Journal*, Vol. 31, 1993, pp. 1191-1198.
- ⁴ Shih, T.-H. and Lumley, J. L., "Kolmogorov behavior of near-wall turbulence and its application in turbulence modeling," NASA TM 105663.
- ⁵ Bardina, J., Ferziger, J. H., and Reynolds, W. C., "Improved turbulence models based on large eddy simulation of homogeneous, incompressible, turbulent flows," Rept. No. TF-19, Stanford University, Stanford, CA., 1983.
- ⁶ Lumley, J. L., "Some comments on turbulence," *Phys. Fluids*, Vol. 4, 1992, pp.203-211.
- ⁷ Reynolds, W.C., 1987, "Fundamentals of turbulence for turbulence modeling and simulation," Lecture Notes for Von Karman Institute, Agard Report No. 755.
- ⁸ Shih, T.-H., Zhu, J., and Lumley, J. L. , "A new Reynolds stress algebraic equation model," NASA TM, 1994, to appear.
- ⁹ Tennekes, H. and Lumley, J. L., *A First Course in Turbulence*, The MIT press (1972).
- ¹⁰ M.S. Mohamed and J.C. Larue, "The decay power law in grid-generated turbulence,"

Journal of Fluid Mechanics, Vol. 219, 1990, pp.195-214.

- ¹¹ Tavoularis, S. and Corrsin, S., "Experiments in nearly homogeneous turbulent shear flow with a uniform mean temperature gradient," *Journal of Fluid Mechanics*, Vol. 104, 1981, pp.311-347.
- ¹² Patel, R. P., "An experimental study of a plane mixing layer," *AIAA Journal*, Vol. 29, 1973, pp.67-71.
- ¹³ Gutmark, E. and Wygnanski, I., "The planar turbulent jet," *Journal of Fluid Mechanics*, Vol. 73, 1976, pp.465-495,
- ¹⁴ Bradbury, L. J. S., "The structure of the self-preserving jet," *Journal of Fluid Mechanics*, Vol. 23, 1965, pp.31-64.
- ¹⁵ Hekestad, G., "Hot-wire measurements in a plane turbulent jet," *Journal of Fluid Mechanics*, Vol. 32, 1965, pp.721-734.
- ¹⁶ Wygnanski, I. and Fiedler, H. E., "The two dimensional mixing region," *Journal of Fluid Mechanics*, Vol. 41, 1970, pp.327-361.
- ¹⁷ Rodi, W., "A new method of analyzing hot-wire signals in highly turbulent flow and its evaluation in round jets," *Disa Information* 1975, No. 17.
- ¹⁸ Kim, J., private communication.
- ¹⁹ Wieghardt, K., "Equilibrium boundary layer at constant pressure," *Computation of Turbulent Boundary Layers-1968 AFSOR-IFP-Stanford University*, Coles, D. E. and Hirst, E. A. ed., Vol. 2, pp.98-123.
- ²⁰ Herring, H. and Norbury, J., "Equilibrium boundary layer in mild negative pressure gradient," *Computation of Turbulent Boundary Layers-1968 AFSOR-IFP-Stanford University*, Coles, D. E. and Hirst, E. A. ed., Vol.2, pp.249-258.
- ²¹ Bradshaw, P., "Equilibrium boundary layer in moderate positive pressure gradient," *Computation of Turbulent Boundary Layers-1968 AFSOR-IFP Stanford University*,

Coles, D. E. and Hirst, E. A. ed., Vol.2, pp.241-248.

- 22 Samuel, A.E., and Joubert, P.N., "A boundary Layer Developing in an Increasingly Adverse Pressure Gradient," *Journal of Fluid Mechanics*, Vol. 66, 1974, pp.481-505.
- 23 Driver, D. M. and Seegmiller, H. L., "Features of a reattaching turbulent shear layer in divergent channel flow", *AIAA Journal*, Vol.23, 1985, pp.163-171.
- 24 Kim, J., Kline, S. J. and Johnston, J. P., "Investigation of separation and reattachment of a turbulent shear layer: Flow over a backward-facing step", Rept. MD-37, Thermosciences Div., Dept. of Mech. Eng., Stanford University, 1978.
- 25 Zhu, J., "A low diffusive and oscillation-free convection scheme", *Comm. App. Num. Methods.*, Vol.7, 1991, pp.225-232.
- 26 Launder, B. E. and Spalding, D. B., "The numerical computation of turbulent flows", *Comput. Meths. App. Mech. Eng.*, Vol.3, 1974, pp.269-289.
- 27 Launder, B. E., Reece, G. J., and Rodi, W., "Progress in the Development of a Reynolds-stress Turbulence Closure," *Journal of Fluid Mechanics*, Vol 68, 1974, pp. 537-566.

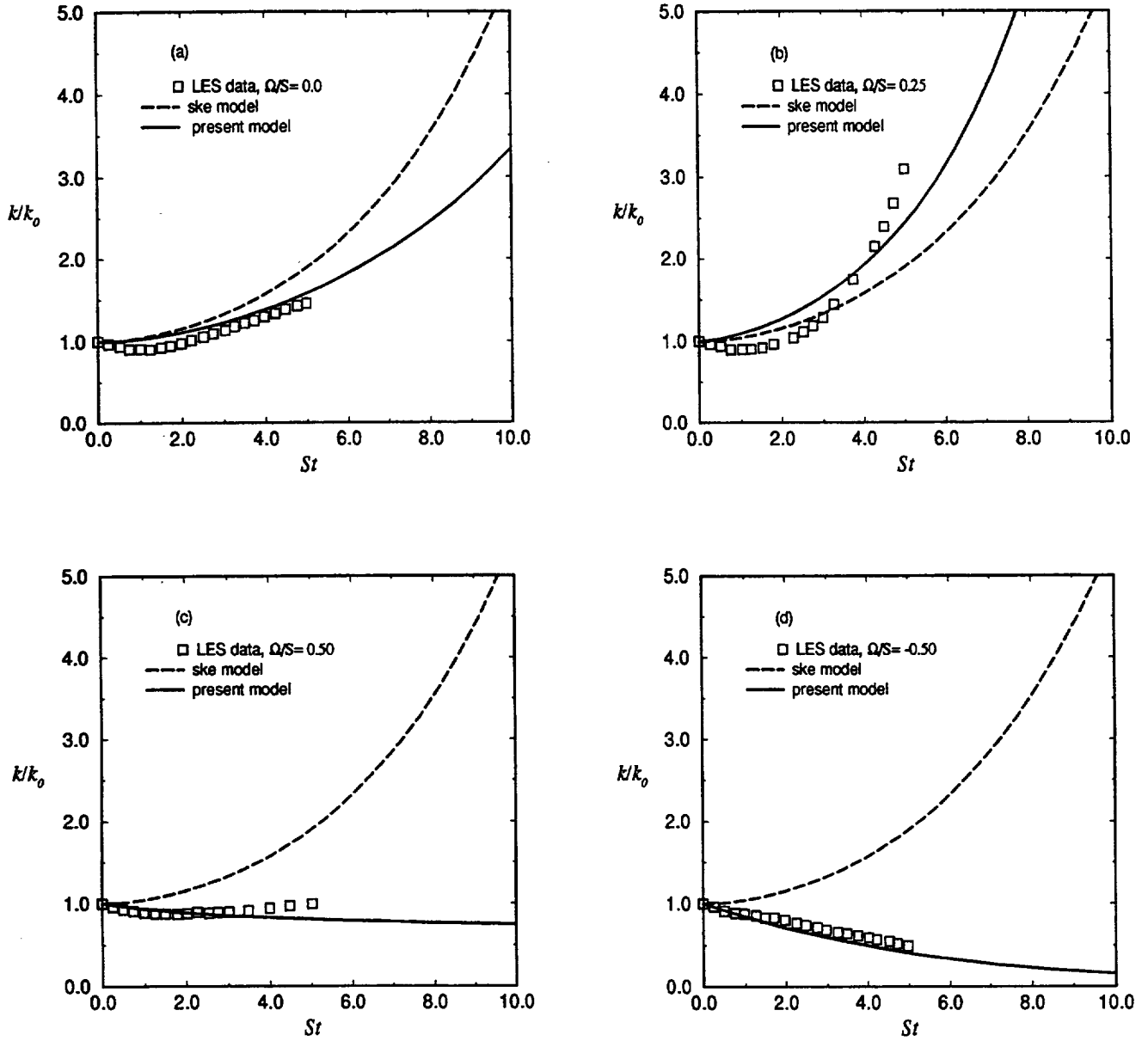


Figure 1. Time evolution of normalized turbulence kinetic energy in various rotating homogeneous shear flows.

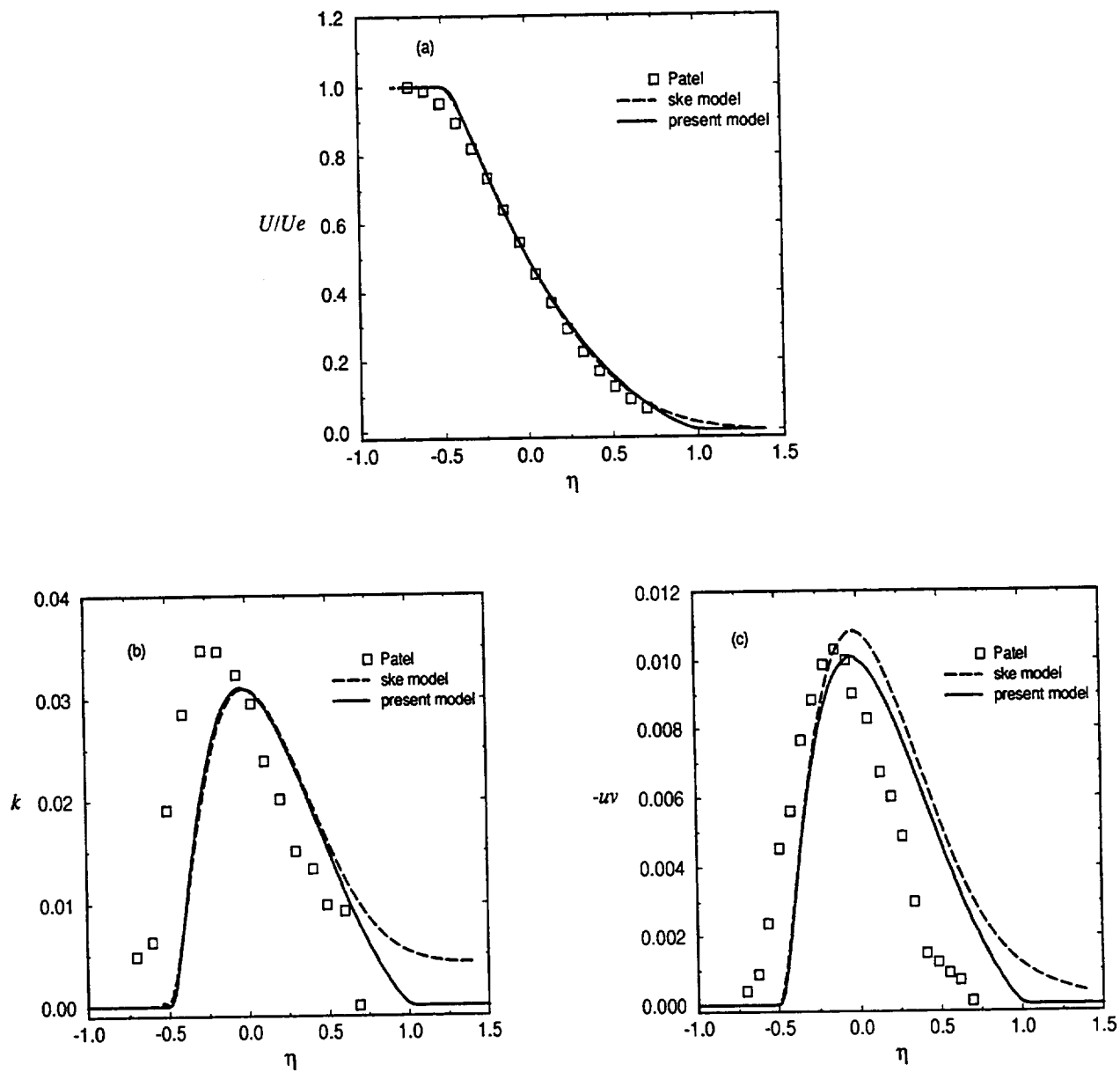


Figure 2. Self-similar profiles for a plane mixing layer. (a) mean velocity; (b) turbulent kinetic energy; (c) Reynolds shear stress.

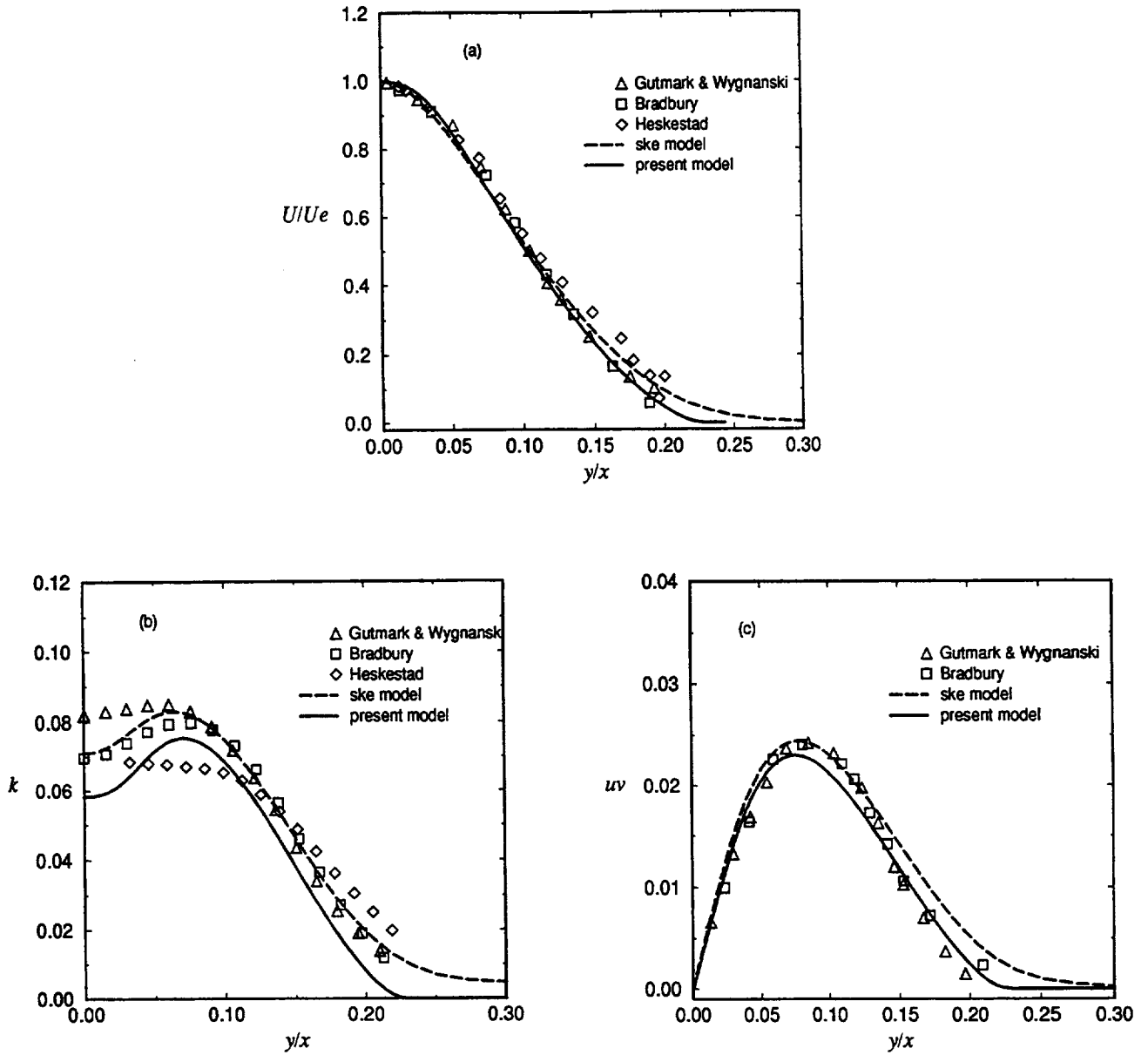


Figure 3. Self-similar profiles for a plane jet. (a) mean velocity; (b) turbulent kinetic energy; (c) Reynolds shear stress.

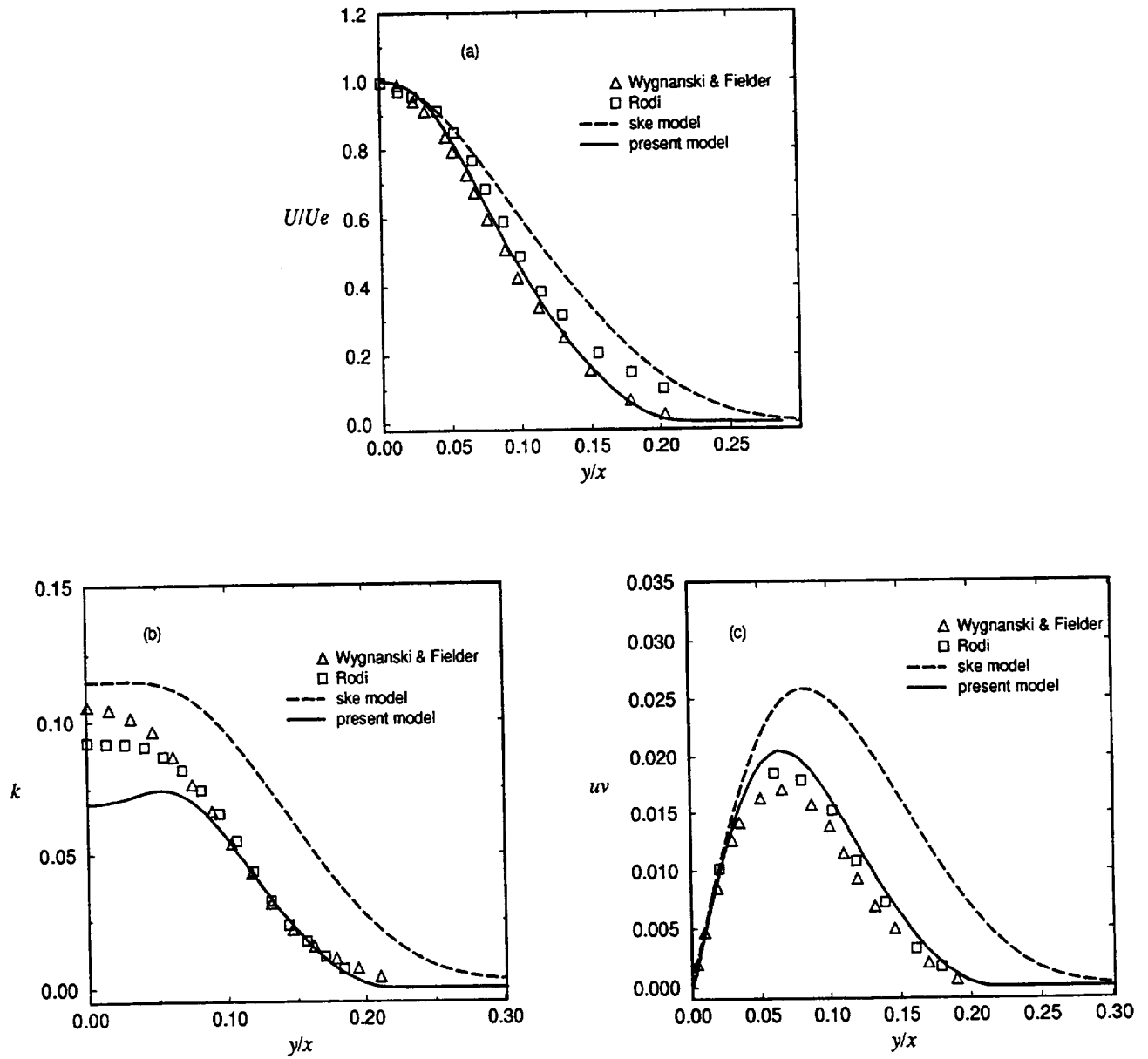


Figure 4. Self-similar profiles for a round jet. (a) mean velocity; (b) turbulent kinetic energy; (c) Reynolds shear stress.

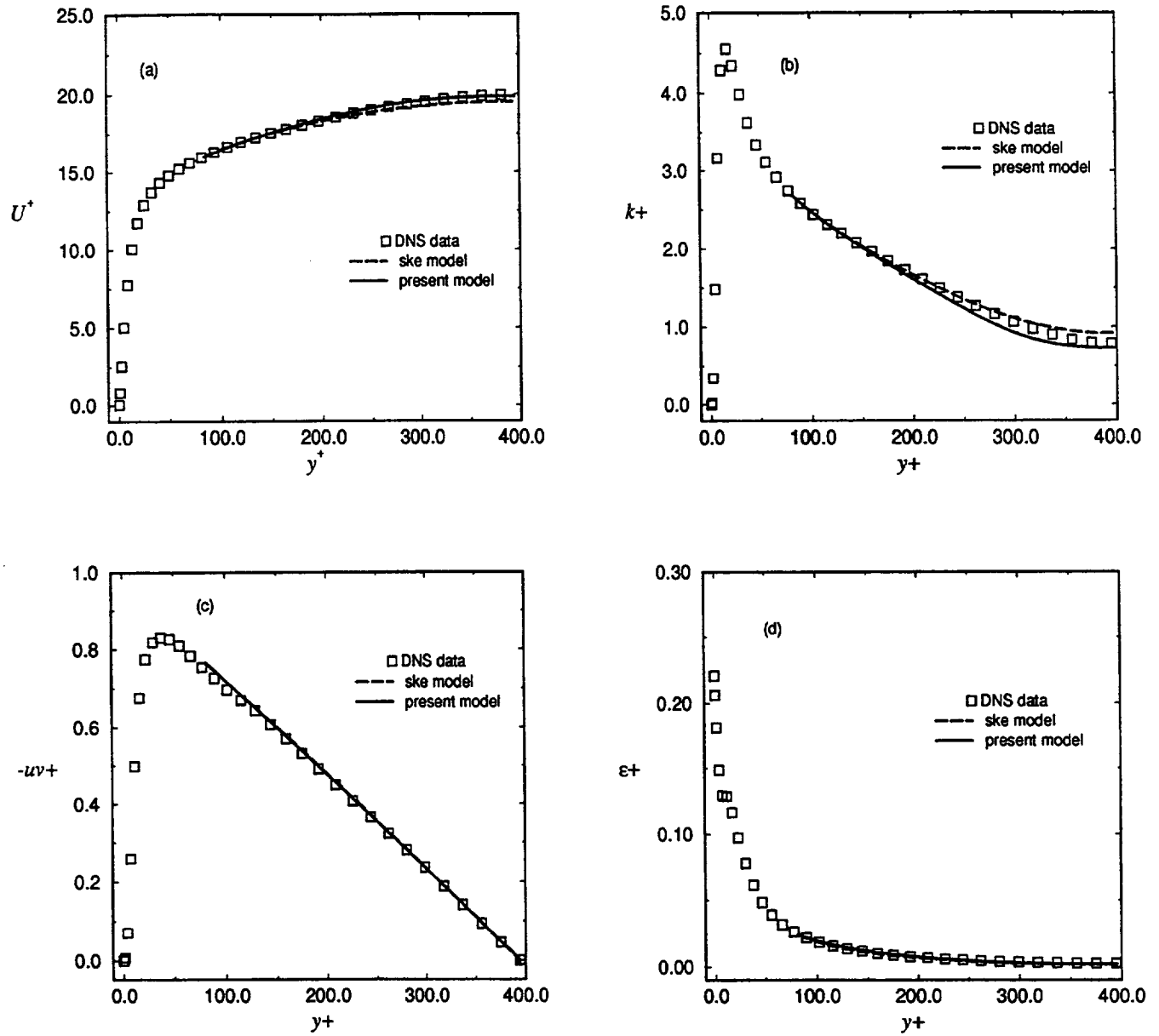


Figure 5. Turbulent channel flow at $Re_\tau = 395$. (a) mean velocity; (b) turbulent kinetic energy; (c) turbulent shear stress; (d) dissipation rate.

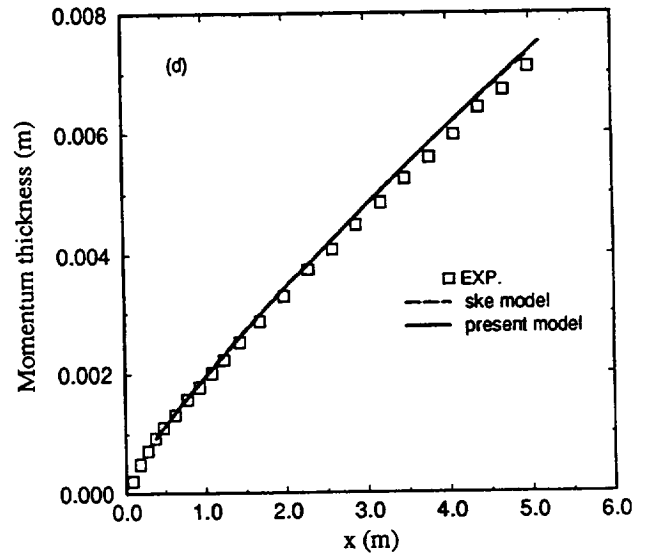
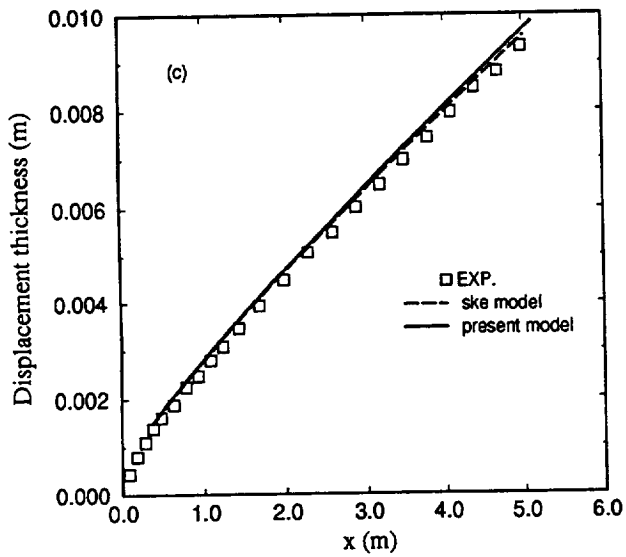
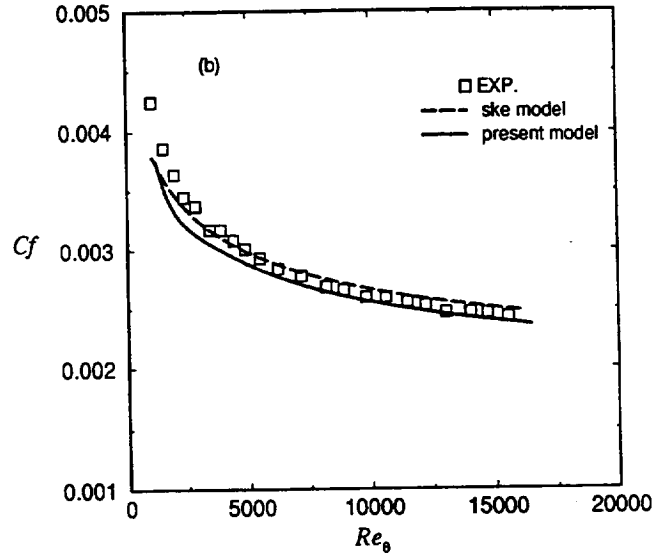
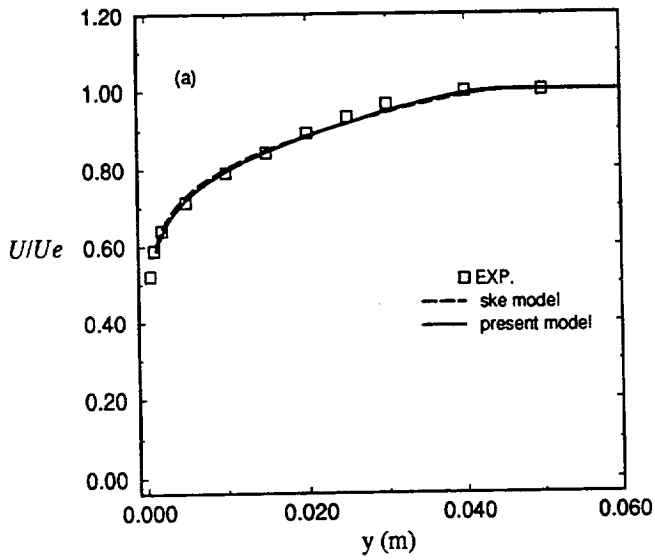


Figure 6. Zero pressure gradient turbulent boundary layer. (a) mean velocity at $Re_\theta=8900$; (b) skin friction coefficient; (c) displacement thickness; (d) momentum thickness.

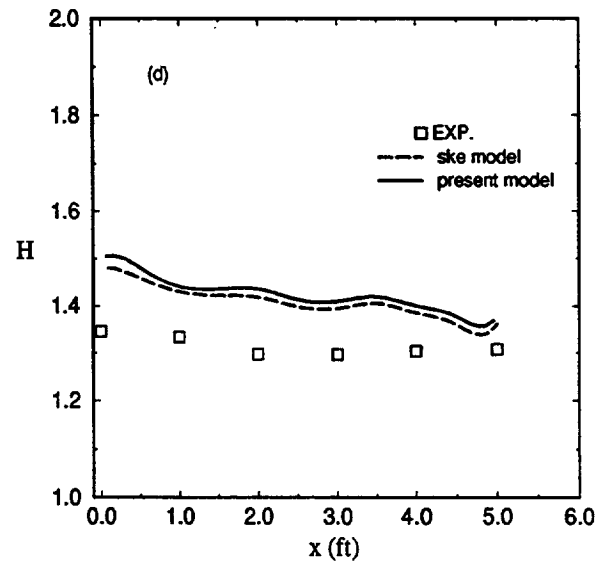
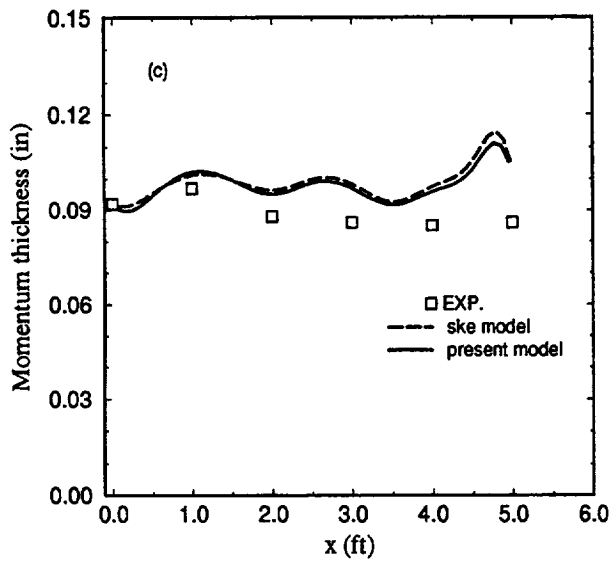
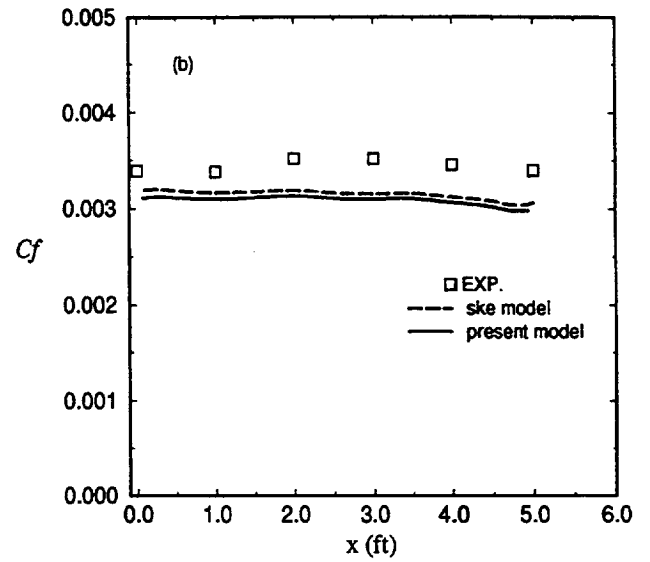
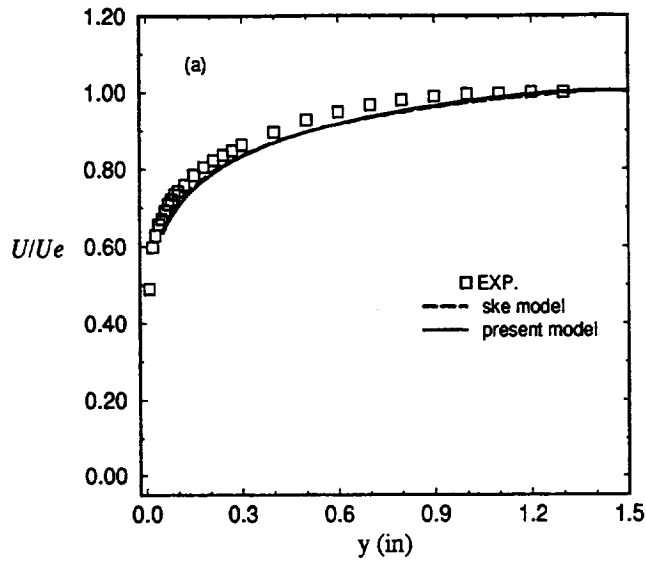


Figure 7. Favorable pressure gradient turbulent boundary layer (Herring and Norbury flow). (a) mean velocity at $x=4.0$ ft.; (b) skin friction coefficient; (c) momentum thickness; (d) shape factor.

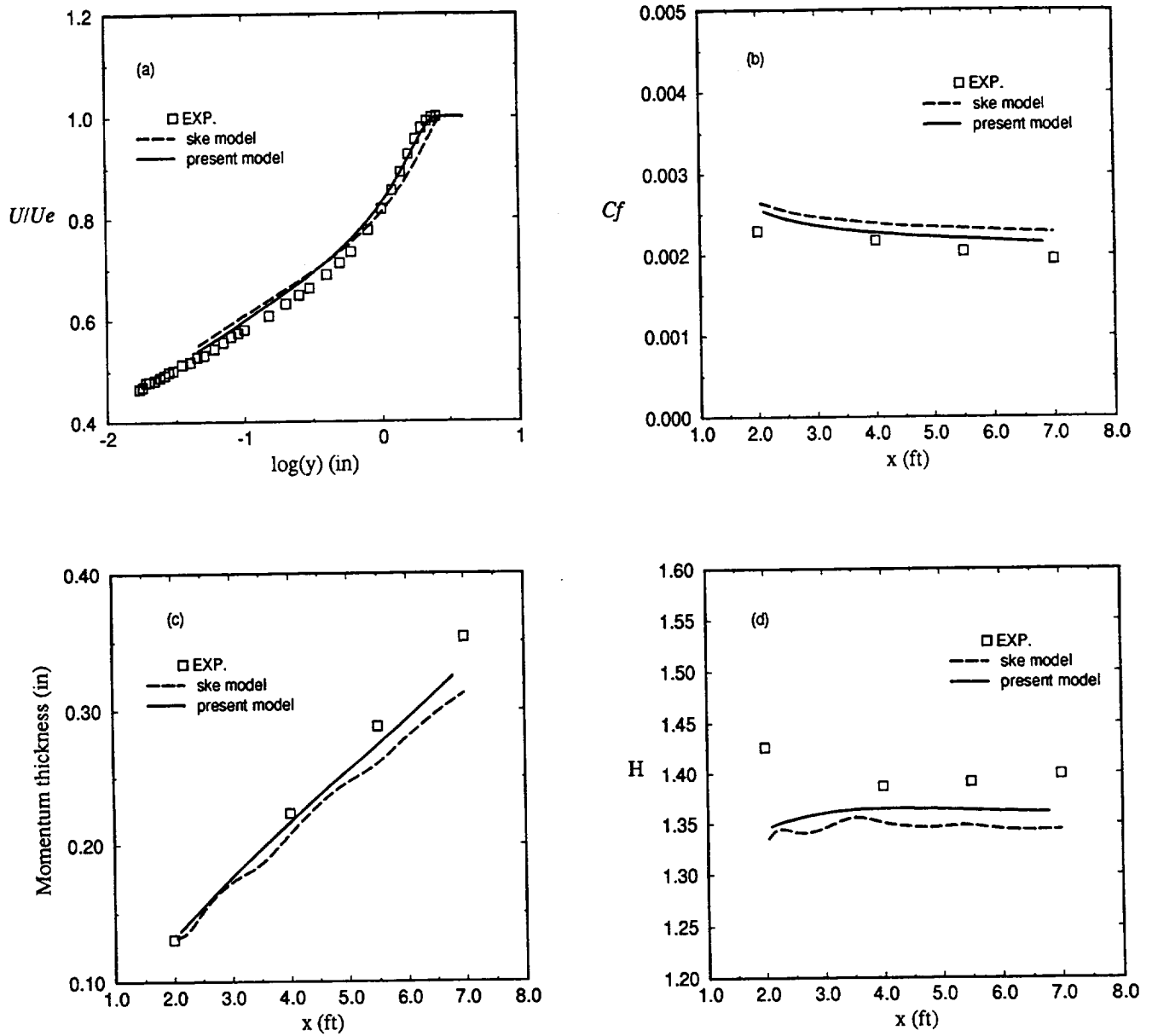


Figure 8. Adverse pressure gradient turbulent boundary layer (Bradshaw flow). (a) mean velocity at $x=5.5$ ft.; (b) skin friction coefficient; (c) momentum thickness; (d) shape factor.

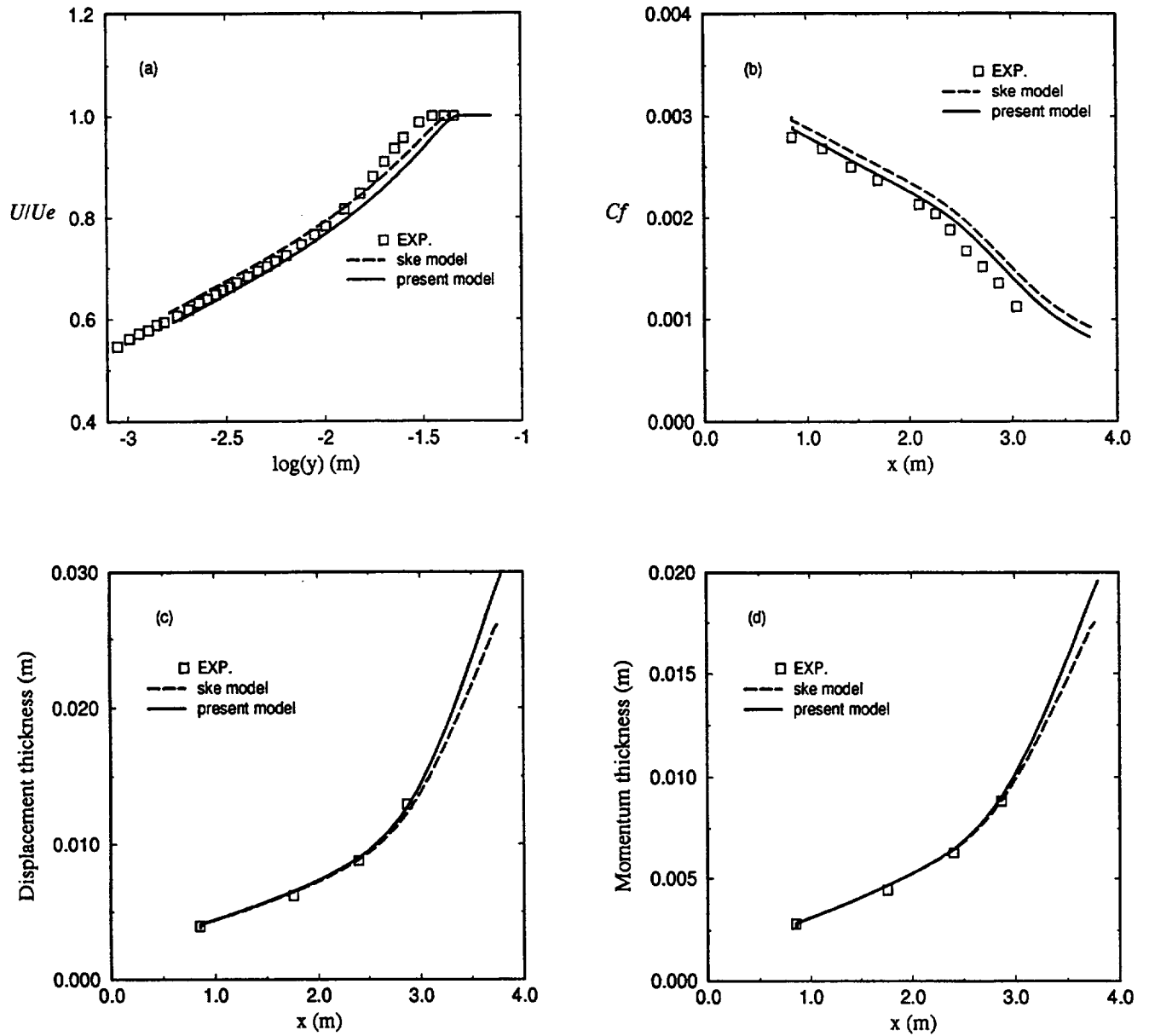


Figure 9. Adverse pressure gradient turbulent boundary layer (Samuel and Joubert flow). (a) mean velocity at $x=1.76$ m.; (b) skin friction coefficient; (c) displacement thickness; (d) momentum thickness.

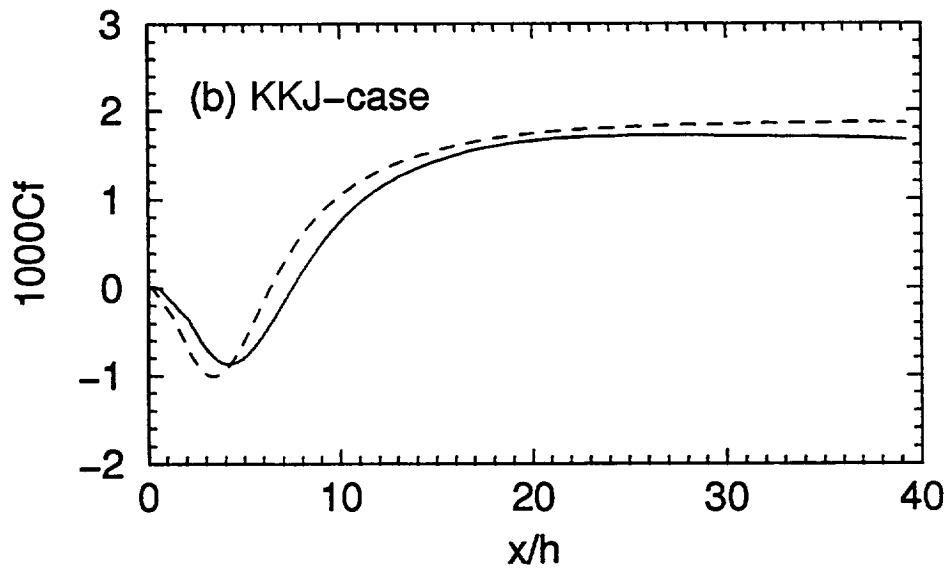
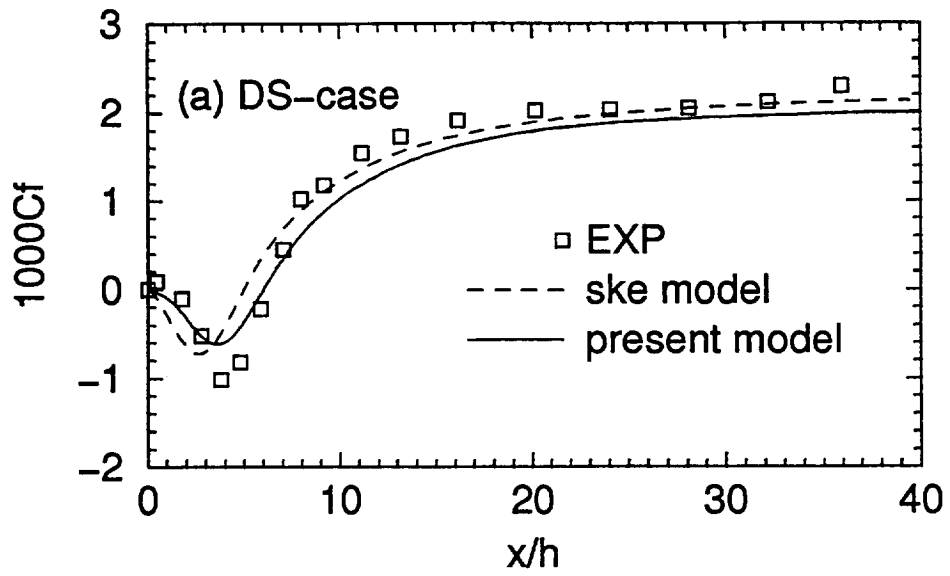


Figure 10. Friction coefficient along the bottom wall

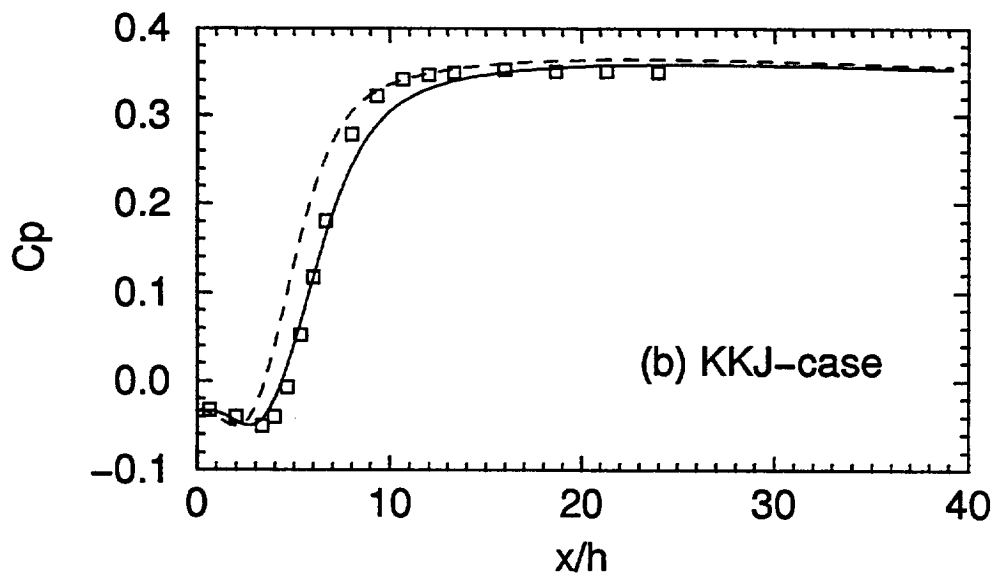
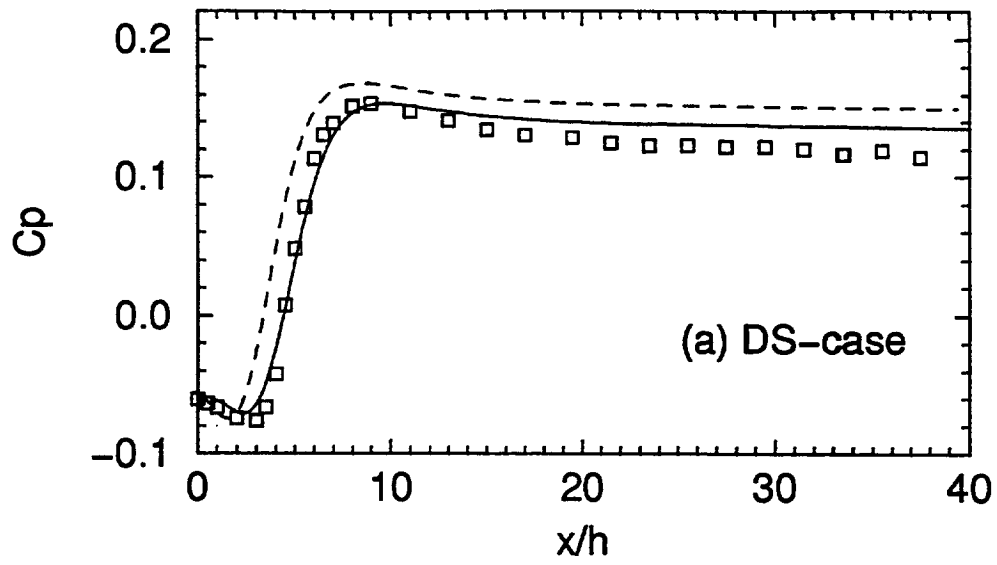


Figure 11. Static pressure coefficient along the bottom wall
(legend as in figure 10)

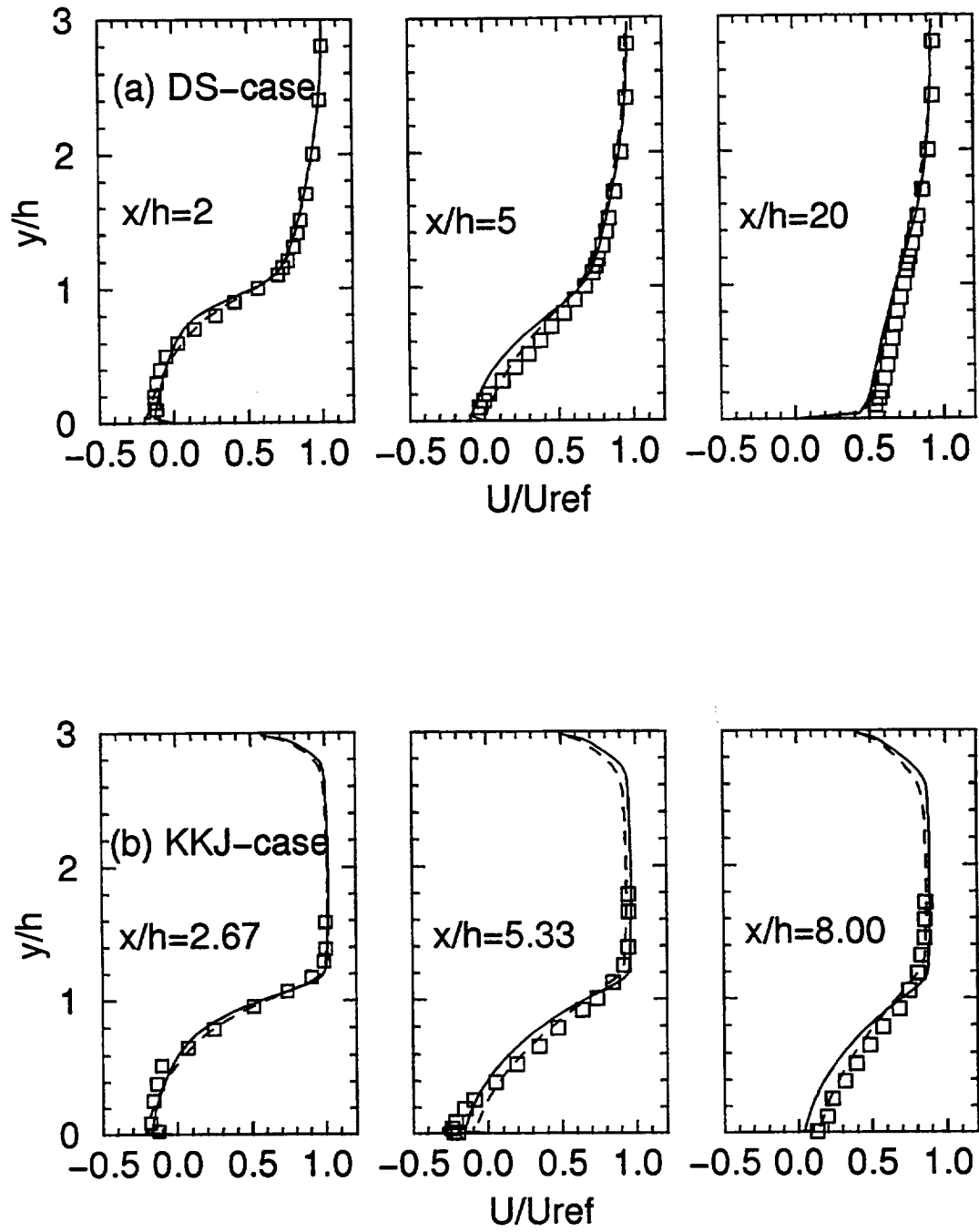


Figure 12. Streamwise mean velocity U -profiles
(legend as in figure 10)

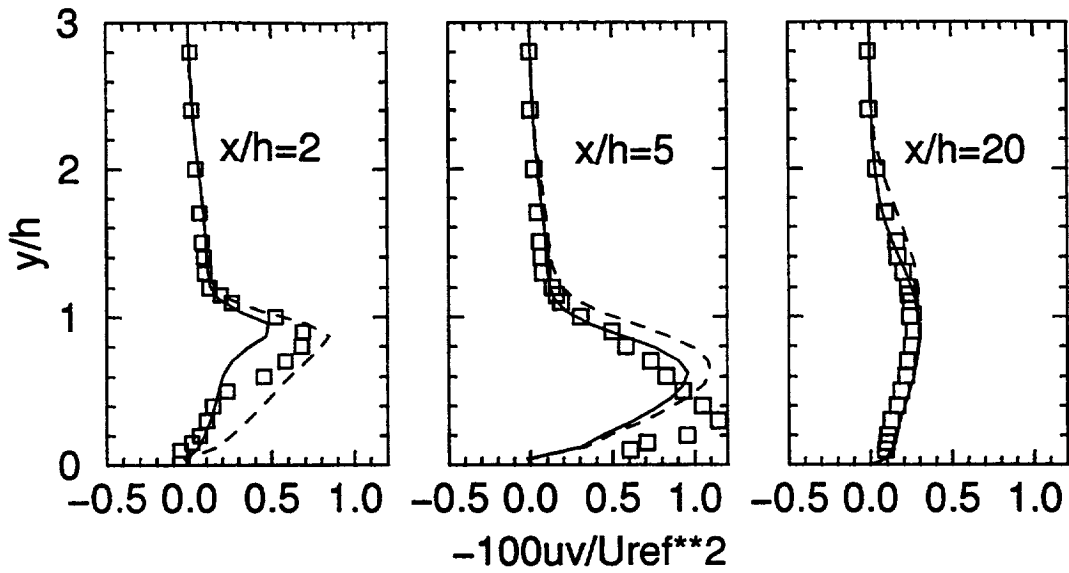


Figure 13. Turbulent shear stress profiles in the DS-case
(legend as in figure 10)

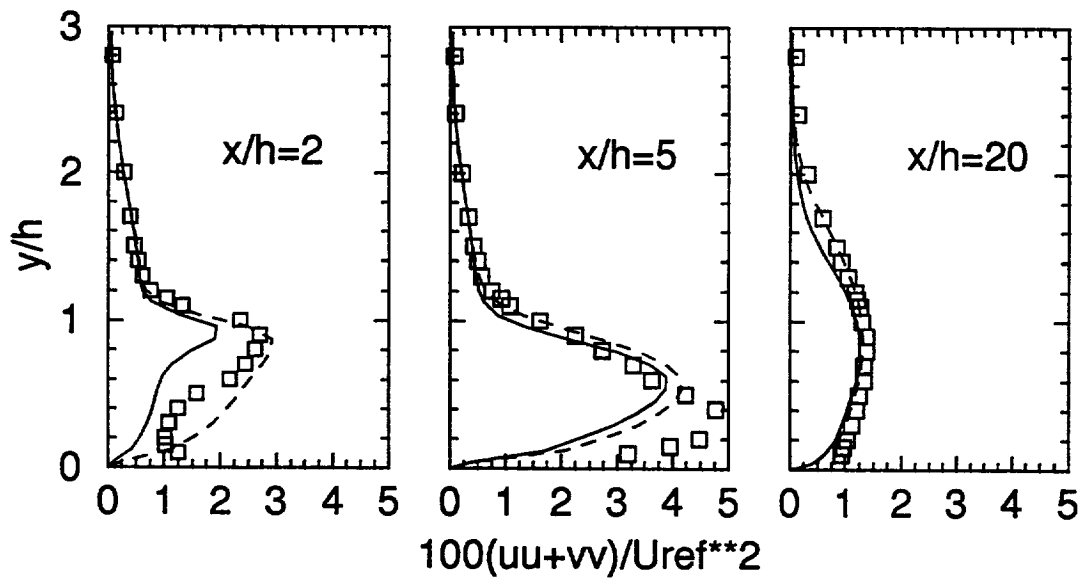


Figure 14. Turbulent normal stress profiles in the DS-case
(legend as in figure 10)

REPORT DOCUMENTATION PAGE

Form Approved
OMB No. 0704-0188

Public reporting burden for this collection of information is estimated to average 1 hour per response, including the time for reviewing instructions, searching existing data sources, gathering and maintaining the data needed, and completing and reviewing the collection of information. Send comments regarding this burden estimate or any other aspect of this collection of information, including suggestions for reducing this burden, to Washington Headquarters Services, Directorate for Information Operations and Reports, 1215 Jefferson Davis Highway, Suite 1204, Arlington, VA 22202-4302, and to the Office of Management and Budget, Paperwork Reduction Project (0704-0188), Washington, DC 20503.

1. AGENCY USE ONLY (Leave blank)	2. REPORT DATE August 1994	3. REPORT TYPE AND DATES COVERED Technical Memorandum	
4. TITLE AND SUBTITLE A New $k-\epsilon$ Eddy Viscosity Model for High Reynolds Number Turbulent Flows—Model Development and Validation		5. FUNDING NUMBERS WU-505-90-5K	
6. AUTHOR(S) T.-H. Shih, W.W. Liou, A. Shabbir, Z. Yang, and J. Zhu			
7. PERFORMING ORGANIZATION NAME(S) AND ADDRESS(ES) National Aeronautics and Space Administration Lewis Research Center Cleveland, Ohio 44135-3191		8. PERFORMING ORGANIZATION REPORT NUMBER E-9087	
9. SPONSORING/MONITORING AGENCY NAME(S) AND ADDRESS(ES) National Aeronautics and Space Administration Washington, D.C. 20546-0001		10. SPONSORING/MONITORING AGENCY REPORT NUMBER NASA TM-106721 ICOMP-94-21 CMOTT-94-6	
11. SUPPLEMENTARY NOTES T.-H. Shih, W.W. Liou, A. Shabbir, Z. Yang, and J. Zhu, Institute for Computational Mechanics in Propulsion and Center for Modeling of Turbulence and Transition, NASA Lewis Research Center (work funded under NASA Cooperative Agreement NCC3-233). ICOMP Program Manager, Louis A. Povinelli, organization code 2600, (216) 433-5818.			
12a. DISTRIBUTION/AVAILABILITY STATEMENT Unclassified - Unlimited Subject Category 34		12b. DISTRIBUTION CODE	
13. ABSTRACT (Maximum 200 words) A new $k-\epsilon$ eddy viscosity model, which consists of a new model dissipation rate equation and a new realizable eddy viscosity formulation, is proposed in this paper. The new model dissipation rate equation is based on the dynamic equation of the mean-square vorticity fluctuation at large turbulent Reynolds number. The new eddy viscosity formulation is based on the realizability constraints; the positivity of normal Reynolds stresses and Schwarz' inequality for turbulent shear stresses. We find that the present model with a set of unified model coefficients can perform well for a variety of flows. The flows that are examined include: (i) rotating homogeneous shear flows; (ii) boundary-free shear flows including a mixing layer, planar and round jets; (iii) a channel flow, and flat plate boundary layers with and without a pressure gradient; and (iv) backward facing step separated flows. The model predictions are compared with available experimental data. The results from the standard $k-\epsilon$ eddy viscosity model are also included for comparison. It is shown that the present model is a significant improvement over the standard $k-\epsilon$ eddy viscosity model.			
14. SUBJECT TERMS Turbulence modeling		15. NUMBER OF PAGES 32	
		16. PRICE CODE A03	
17. SECURITY CLASSIFICATION OF REPORT Unclassified	18. SECURITY CLASSIFICATION OF THIS PAGE Unclassified	19. SECURITY CLASSIFICATION OF ABSTRACT Unclassified	20. LIMITATION OF ABSTRACT